Gally, C.; García Gabaldón, M.; Ortega Navarro, EM.; Bernardes, A.; Pérez-Herranz, V. (2020). Chronopotentiometric study of the transport of phosphoric acid anions through an anion-exchange membrane under different pH values. Separation and Purification Technology. 238:1-10. https://doi.org/10.1016/j.seppur.2019.116421

Chronopotentiometric study of the transport of phosphoric acid anions through an anion-exchange membrane under different pH values.

C. Gally[1,2]; M. García-Gabaldón[1]; E.M. Ortega[1]; A.M. Bernardes[2,*], V. Pérez-Herranz[1].

[1]Grupo IEC, Departamento de Ingeniería Química y Nuclear, E.T.S.I. Industriales, Universitat Politècnica de València, POBox 22012, E-46022 València, Spain

[2]LACOR, PPGE3M, Universidade Federal do Rio Grande do Sul, Av. Bento Gonçalves, 9500, Setor 4, Prédio 43426, Campus do Vale, 91509-900 Porto Alegre, RS, Brazil

*Corresponding author. e-mail address: amb@ufrgs.br

Abstract.

Phosphate is the main cause of eutrophication in many water bodies. Its presence in waters is associated to the fact that is not completely removed in conventional wastewater treatment plants. On the other side, phosphate rocks are a non-renewable resource and considered as a critical raw material. A membrane separation process, able to recover phosphate from wastewater, is a promising process to avoid pollution and to reuse phosphate. This paper investigates the transport of salts of phosphoric acid through an anion-exchange membrane (AEM) by means of chronopotentiograms and polarization curves (CVCs).

The presence of multiple transition times in the chronopotentiograms and the corresponding limiting current densities in the CVCs indicate a change in the species being transported in the membrane/diffusion boundary layer system, due to the hydrolysis reactions that take place when the concentration polarization is reached. Under the experimental conditions tested, coupled convection (gravitational and elctroconvection) occurs when a certain threshold in the membrane voltage drop is surpassed independently of the electrolyte concentration. However, at high pH values, only one transition time in the chronopotentiograms, due to the transfer of OH^- ions with greater concentration and mobility. This fact is reflected in the CVCs by the large plateaus obtained, which hinders the occurrence of coupled convection phenomena, and consequently, water splitting can be considered as the main mechanism responsible for the overlimiting regime.

Keywords: Anion exchange membranes; Phosphoric acid salts; Chronopotentiometry; Current–voltage characteristics; Hydrolysis

1. Introduction.

Phosphorus is a key ingredient in fertilizers composition to keep high efficiency of crops and in the industry related with food production. During the last decades, its use has increased continuously, and it is expected that this trend will continue in the future. Since phosphorus production is based on phosphate rock, its consumption will lead to depletion of a non-renewable resource and will inevitably become increasingly expensive [1–3]. Reducing its use is beneficial not only from the view point of preserving the phosphorus reserves, but also for the removal of phosphates from wastewaters and livestock waste. In this sense, its recovery from wastewater would minimize eutrophication with the consequent improvement that this entails in the wastewater treatment plants [4,5].

Different technologies have been proposed to remove and recover phosphate from wastewater, such as chemical precipitation, adsorption, membrane filtration or biological processes [6–13]. Among all of these techniques, struvite crystallization has managed to attract a lot of attention because it allows phosphate and ammonia simultaneous recovery [14–16]. However, this method is less effective in reducing salinity and also, the waste generated in the precipitation technique has to be managed. On the other hand, the high salinity present in wastewater, that affects the regeneration costs of the resins, limits the application of the adsorption technique.

In order to solve these problems, novel processes able to remove P and reduce the salinity of the wastewater must be developed with the aim of reaching the zero-liquid discharge of the effluents [17]. Recently, electrochemical techniques such as capacitive deionization [18–20] and electrodialysis [11,17,21] have been proposed for phosphate removal and recovery. Electrodialysis would be an alternative technique to directly recover and concentrate phosphorous in the form of orthophosphate ($H_xPO_4^{x-3}$) and can also reduce biological activity [22]. However, as phosphate salts are weak electrolytes, depending on the pH, orthophosphate ions may exist in the form of dihydrophosphate, hydrophosphate- and phosphate- ions.

Understanding the transport mechanisms of solutions containing weak electrolytes through ion-exchange membranes is of great interest [23], as weak electrolytes can give rise to certain problems related to their small degree of dissociation, their competition with strong electrolyte ions or the occurrence of hydrolysis reactions coupled with the transport. On the other hand, under currents exceeding the limiting current density, water splitting can take place at the membrane/solution interface. This fact affects the hydrolysis degree of the species and complicates the interpretation of the obtained results [24]. Therefore, the knowledge of the transport of phosphate-containing

solutions through ion-exchange membranes is of great importance for the recovery of phosphate by electrodialysis and it has been the object of several studies [25–29].

Chronopotentiometry is an electrochemical technique useful to identify different phenomena taking place in interfacial processes [30–32], and has been applied to evaluate the transport properties of different ions through ion-exchange membranes (IEMs) [33–35]. This technique provides interesting data regarding with membrane heterogeneity, electric conductivity, permselectivity and transport numbers. Moreover, it represents an indirect measurement of the changes in the solution composition taking place at the membrane/solution interface and helps to the understanding of the phenomena occurring as a consequence of the concentration polarization phenomena (water splitting, gravitational convection and electroconvection), fouling and scaling.

Current-voltage curves (CVCs) are obtained from the constant values of the membrane potential drop when the stationary state is reached in the chronopotentiograms, and are frequently employed to study the transport of the different species through the ion-exchange membranes. The typical shape of these curves shows three different regions: a quasi-linear region known as ohmic region, a horizontal area corresponding to the limiting current conditions, and an overlimiting region, associated with water splitting, electroconvection and gravitational convection [36]. From the CVCs, parameters as the resistance of the ohmic region and the plateau length could also be obtained.

This paper deals with the investigation of the transport of phosphate ions through an anion-exchange membrane using chronopotentiometry and current-voltage curves. The application of these techniques to the study of phosphate ion transport will make possible to select the adequate conditions for the recovery of phosphate through electrodialysis. The novelty of this paper lies in the lack of bibliographic information about the transport of weak electrolyte anions through anionic exchange membranes. In this sense, the elaboration of speciation diagrams of the species as a function of pH is necessary for a better understanding of the transport phenomena across the membrane.

2. Experimental.

2.1. Membranes.

The membranes employed in this work were provided by Hidrodex®. The cation-exchange membrane (CEM) had sulfonic acid groups as fixed ion-exchange sites, while the anion-exchange membrane (AEM) had quaternary amine groups as fixed ion exchange sites. Both membranes are heterogeneous with a reinforced structure to increase the mechanical resistance. Their main characteristics are shown in Table 1. The study of the transport of $H_xPO_4^{x-3}$ ions through the AEM is the objective of this work, and the CEM served to avoid the presence of the OH^- ions generated at the cathode in the proximities of the AEM. Before each experimental test, the membranes were immersed under stirring in the solution of the same concentration as that required in the experiments during 24 h.

Table 1. Characteristics of cationic (CEM) and anionic (AEM) membranes

Parameter	Unit	(CEM)	(AEM)
Water Containment	%	35-50	30-45
Ionic Exchange Capacity	$mol.kg^{-1}$ (dry)	≥2.0	≥1.8
Surface resistance of the membrane (0.1 mol NaCl)	$Ohm.cm^{-2}$	≤20	≤20
Shear strength	MPa	≥0.6	≥0.6
Degree of expansion	%	≤2	≤2
Water Permeability	$mL.h.cm^{-2}$	≤0.1 (below 0.2 MPa)	≤0.2 (below 0.035 MPa)

2.2. Reagents.

The study was performed with synthetic solutions containing different concentrations of H_3PO_4, Na_2HPO_4, Na_3PO_4 and NaCl. The pH was adjusted with a NaOH 50% w/w solution. Analytical grade reagents were purchased from Panreac.

2.3. Experimental setup

The experimental setup, which is well described in previous works [30,31], consisted on three cylindrical compartments with the AEM and the CEM clamped between them. Each compartment had a volume of 130 ml and the effective area of the membranes was 3.14 cm^2. Both membranes were circular-shaped and the intermediate distance between them was 6 cm. Tests were performed in duplicate, at room temperature and under static conditions without recirculation.

Different current pulses, with duration of 300 seconds, were imposed. Then, the current pulse was switched off during a relaxation stage of 100 additional seconds before a new incremented current pulse. The response of the membrane voltage drop was registered and CVC curves were also obtained in potentiodynamic mode.

3. Results and discussion.

In aqueous solutions of orthophosphate salts, the following chemical reactions can be considered:

$$H_3PO_4 \rightleftarrows H_2PO_4^- + H^+ \qquad K_{a1} = \frac{[H_2PO_4^-][H^+]}{[H_3PO_4]} = 10^{-2.15} \tag{1}$$

$$H_2PO_4^- \rightleftarrows HPO_4^{2-} + H^+ \qquad K_{a2} = \frac{[HPO_4^{2-}][H^+]}{[H_2PO_4^-]} = 10^{-7.2} \tag{2}$$

$$HPO_4^{2-} \rightleftarrows PO_4^{3-} + H^+ \qquad K_{a3} = \frac{[PO_4^{3-}][H^+]}{[HPO_4^{2-}]} = 10^{-12.38} \tag{3}$$

The equation system formed by equations (1) to (3), the mass balance for phosphate and the ionic product of water given by equations (4) and (5) respectively, and the proton balance for each solution, served us to estimate the concentration of the different species present in equilibrium (table SM-1 of the Supplementary Material) and to elaborate the speciation diagrams.

$$C_0 = [H_3PO_4] + [H_2PO_4^-] + [HPO_4^{2-}] + [PO_4^{3-}] \tag{4}$$

$$H_2O \rightleftarrows H^+ + OH^- \qquad K_w = [H^+][OH^-] = 10^{-14} \tag{5}$$

The speciation diagrams of phosphate ions are presented in Figure SM-1 (supplementary material), where the predominance of each species as a function of pH is shown. According to the calculated equilibrium pH, and considering the species that predominate at those pH values, the solutions have been classified into 6 different groups (see Fig. SM-1). At pH values between 4.79 and 5.10, solutions IV and XI, $H_2PO_4^-$ ions predominate. At pH 6.36, solution IX, the predominant species are $H_2PO_4^-$ and HPO_4^{2-}, with a higher concentration of $H_2PO_4^-$. In solutions III, XIII, XV, XVI and XVII, with pH values between 7.20 and 7.30, $H_2PO_4^-$ and HPO_4^{2-} have approximately the same concentration. In solutions I, II, V, X and XII, with pH values between 9.10 and 10.40, HPO_4^{2-} is the predominant species. At pH values between 12.26 and 12.44, solutions VI and VII, the predominant species are HPO_4^{2-} and PO_4^{3-}, with the highest concentration of HPO_4^{2-}. Finally, at pH 13, solutions VIII and XIV, HPO_4^{2-} and PO_4^{3-} also predominate, but the concentration of PO_4^{3-} is greater.

3.1. Effect of Na_2HPO_4 concentration on the chronopotentiograms and the CVCs.

For this initial study, three different concentrations of Na_2HPO_4 without the addition of other compounds were employed (Solutions I, II and X). As shown in Table 2, these solutions had pH values of 9.85, 9.56 and 9.10 respectively, and the main components in equilibrium conditions were HPO_4^{2-} and Na^+, as observed in Table SM-1 (supplementary material).

Table 2. pH, conductivity and CVCs characteristics of the working solutions as a function of the Na_2HPO_4 concentration.

Soln ID	$[Na_2HPO_4]$ ($mol \cdot L^{-1}$)	pH	κ ($\Omega^{-1} \cdot cm^{-1}$)	R1 ($\Omega \cdot cm^2$)	i_{lim} ($A \cdot cm^{-2}$)	$I_{plateau}$ (V)
I	0.1	9.85	$2.15 \cdot 10^{-2}$	59.9	$2.39 \cdot 10^{-2}$	1.50
II	0.01	9.56	$2.15 \cdot 10^{-3}$	330	$1.06 \cdot 10^{-3}$	0.75
X	0.001	9.10	$2.16 \cdot 10^{-4}$	6520	$7.03 \cdot 10^{-5}$	0.50

The chronopotentiometric curves had the typical shape described in the literature as shown in Figure SM-2 (supplementary material) for a 0.01 $mol \cdot L^{-1}$ solution of Na_2HPO_4 (solution II). The height of the initial vertical part of the curve is the ohmic potential drop (U_{Ohm}), and its slope is related with the capacity of the electrical double layer at the membrane/solution interface [37,38]. At these low values of applied current, the polarized membrane acts as a resistance to the transport of current, and the values of the membrane potential, U_m, do not increase too much, as a strong reduction of the counterion concentration at the membrane/solution interface is not already reached. However, at higher applied current densities, a steeper depletion of counterions takes place at the membrane surface on the dilute side, governed mainly by electro-diffusion processes. In this case, a steep increase in U_m appears in the chronopotentiogram due to the resistance of the diffusion boundary layer, and an inflection point that defines the transition time (τ) is reached. This time represents the value at which the interfacial concentration becomes zero, and is calculated from the maximum of the derivative of U_m as observed in Figure SM-2 for 1.6 $mA \cdot cm^{-2}$ [37]. The transition time (τ) for a homogeneous ion-exchange membrane, given by Sand's equation, is used to obtain the ion transport number through the membrane [33–35]:

$$\tau = \left(\frac{\pi \cdot D}{4}\right)\left(\frac{z \cdot F}{T_j - t_j}\right)^2 \left(\frac{C_0}{i}\right)^2 \quad (6)$$

where D is the salt diffusion coefficient, C_0 is the concentration in the bulk and z the charge of the counterion, T_i and t_i are the transport numbers of the counterion in the membrane and in the solution, respectively, i the current density and F is the Faraday's constant.

The limiting current density (i_{lim}) represents the value of current beyond which the inflexion point is observed, and consequently, the mass transfer limitation appears. This parameter can be calculated by means of the Peers' equation [39,40]:

$$i_{lim} = \frac{z \cdot F \cdot D \cdot C_0}{\delta\left(T_j - t_j\right)} \tag{7}$$

For applied currents higher than i_{lim} other transport mechanisms may take place, such as electroconvection, gravitational convection or water splitting. The transition time decreases with the increase in the applied current due to the faster ion depletion in the membrane/solution interface. After the sharp increase in U_m when surpassing τ, the membrane voltage drop keeps approximately constant until the end of the current pulse. During the relaxation stage U_m tends to zero.

Chronopotentiometric curves for 0.1 M Na_2HPO_4 (solution I) behave different as seen in Figure 1. For applied currents higher than $i_{lim,}$ the curves show a maximum in U_m after the transition time. Some authors attribute this behavior to the decrease of the concentration polarization phenomena [37,39,41], mainly caused by different phenomena such as the transfer of co-ions across the membrane, which increases with time during chronopotentiometry, together with the gravitational convection, which can take place in concentrated electrolytes due to the formation of high concentration gradients near the membrane/solution interface in the presence of an electric field, producing a decrease of the thickness of the diffusion boundary layer.

Figure SM-3 (supplementary material) presents the comparison of the chronopotentiograms obtained for the three concentrations of Na_2HPO_4 for the same value of i/C_0 (127 $A \cdot cm \cdot mol^{-1}$). As can be seen, the ohmic potential drop of the membrane/solution interface, U_{Ohm}, has the same value for the three solutions. U_{Ohm} depends on the conductivities of the solution and the membrane, and therefore on the solution ionic concentration. Since in the chronopotentiograms of Figure SM-3 the applied current density is normalized with respect to the electrolyte concentration, U_{Ohm} has the same value for the three solutions. However, after reaching the U_{Ohm} value, the evolution of U_m with time is different for the three solutions. For the most concentrated solution, U_m remains almost constant during the course of the current pulse, since in these conditions, the development of concentration gradients is not achieved. For the most diluted solution, the transition time is clearly observed. The solution composed of 0.01 $mol \cdot L^{-1}$ Na_2HPO_4 exhibited an intermediate behavior.

The CVCs for the same solutions as those presented in the previous chronopotentiograms are presented in Figure 2 (a). In this Figure, the ratio i/C_0 has been represented versus U_m, since, as mentioned previously, i is proportional to the

concentration of each ion present in the solution. The curves show the three characteristic regions previously mentioned [33]: in the first region (ohmic region), the resistance of the system (R1) can be calculated from the inverse of the slope of the straight line that fits this area. In the second region ("plateau" region) small current increments cause a high potential raise due to ion transport limitation from the bulk solution to the boundary layer at high values of i. The i_{lim} parameter previously defined, is determined from the intersection of the first and the second regions as observed in Figure 2 (a). In the third region (overlimiting region), U_m presents a new linear relationship with i. The length of the plateau region ($l_{plateau}$) is the increase of U_m needed to reactivate the transport of species through the membrane and is obtained as shown in Figure 2 (a). It represents the energy input that has to be supplied to a membrane system in order to onset the generation of electroconvective vortices or the gravitational convection [31,33,42]. R1, i_{lim} and $l_{plateau}$ are presented in Table 2 for each solution composition, where it is inferred that in solutions with similar pH, i_{lim} and $l_{plateau}$ increase with the initial concentration of phosphate.

As seen in Figure 2 (a), i_{lim}/C_0 increases with the concentration of Na_2HPO_4, although as predicted by equation (7), this value should remain constant if D, T_j, t_j and δ do not change with the salt concentration. As mentioned previously, for solutions of Na_2HPO_4 at pH of about 9, the main species in solution are Na^+ and HPO_4^{2-} (see Table SM-1), and although the transport number of the counterion in the membrane (t_i) decreases with the salt concentration due to Donnan exclusion, this phenomenon does not justify the increase of i_{lim}/C_0 with the Na_2HPO_4 concentration. This could be explained by the variation of the boundary layer (δ) thickness with the concentration.

Under natural gravitational convection conditions (i.e. membrane in vertical position and no stirring) the thickness of δ depends on the concentration gradient between the bulk solution and the membrane surface as predicts the Levich equation [43]:

$$\delta \approx \frac{L^{1/4}}{0.7Sc^{1/4}(g \cdot \Delta C/4\nu^2)^{1/4}} \quad (8)$$

where L is the membrane height, g the gravity acceleration, Sc =ν/D the Schmidt number, ν kinematic viscosity of the solution, expressed as $\nu = \mu/\rho$ (where μ is the absolute viscosity and ρ the solution density), and ΔC is the gradient concentration in the boundary layer.

Under limiting conditions, ion concentration at the membrane surface is null and ΔC becomes C_0. Hence, according to equations (7) and (8), it is deducted that i_{lim} depends on $C_0^{1.25}$, if in the range of working concentrations (ρ and μ) remain constant.

Figure 2 (b) shows the curves $i/C_0^{1.25}$ versus U_m for the same solutions of those found in Figure 2 (a). As can be observed, when plotting $i/C_0^{1.25}$ versus U_m instead of i/C_0, the same value of $i_{lim}/C_0^{1.25}$ is obtained for all concentrations of Na_2HPO_4. This confirms the effect of the boundary layer thickness on the limiting current density, and can explain also the effect of the Na_2HPO_4 concentration on the chronopotentiograms of Figure SM-3 (supplementary material).

3.2. Effect of pH on the chronopotentiograms and the CVCs.

In contrast with strong electrolytes, the salts of weak-acids participate in hydrolysis reactions, which are reversible processes, and consequently, a variation of pH may affect the concentration of the different ionic forms present at equilibrium. For this reason, the effect of pH on the chronopotentiograms and on the CVCs was studied for two initial concentrations of phosphate salts 0.01 (Table 3) and 0.001 M (Table 4), where the appropriate amount of NaOH was added when necessary.

Table 3. pH, conductivity and CVCs characteristics of the working solutions as a function of the pH for a phosphate concentration of 0.01 M

Soln ID	pH	κ ($\Omega^{-1}\cdot cm^{-1}$)	R1 ($\Omega\cdot cm^2$)	i_{lim} ($A\cdot cm^{-2}$)	$I_{plateau}$ (V)
II	9.56	$2.15\cdot10^{-3}$	330	$1.06\cdot10^{-3}$	0.75
III	7.20	$1.50\cdot10^{-3}$	335	$8.77\cdot10^{-4}$	0.90
IV	4.79	$8.70\cdot10^{-4}$	874	$7.39\cdot10^{-4}$	0.90
V	10.4	$2.22\cdot10^{-3}$	313	$1.40\cdot10^{-3}$	1.70
VI	12.26	$7.62\cdot10^{-3}$	78.7	$7.18\cdot10^{-3}$	2.00
VII	12.44	$1.01\cdot10^{-2}$	57.8	$8.30\cdot10^{-3}$	2.05
VIII	13.01	$2.92\cdot10^{-2}$	17.1	$3.19\cdot10^{-2}$	2.10
IX	6.36	$1.02\cdot10^{-3}$	190	$4.02\cdot10^{-4}$	0.90

Table 4. pH, conductivity and CVCs characteristics of the working solutions as a function of the pH for a phosphate concentration of 0.001 M

Soln ID	pH	κ ($\Omega^{-1}\cdot cm^{-1}$)	R1 ($\Omega\cdot cm^2$)	i_{lim} ($A\cdot cm^{-2}$)	$I_{plateau}$ (V)
X	9.1	$2.16\cdot10^{-4}$	6520	$7.03\cdot10^{-5}$	0.50
XI	5.1	$8.95\cdot10^{-5}$	4272	$1.92\cdot10^{-4}$	0.85
XII	10.25	$2.59\cdot10^{-4}$	2391	$7.97\cdot10^{-5}$	1.45
XIII	7.3	$1.57\cdot10^{-4}$	6402	$1.92\cdot10^{-5}$	0.90
XIV	13.05	$2.82\cdot10^{-2}$	15.3	$3.83\cdot10^{-2}$	2.02

Figure SM-4 (supplementary material) shows the effect of pH on the chronopotentiograms obtained in a 0.01 M phosphate solution for the same value of i (1.6 $mA \cdot cm^{-2}$). Although in these conditions all chronopotentiograms present the typical shape, pH has an important effect on some of their characteristics. With respect to the first part of the curves, when the current is switched on, different values of U_{Ohm} are reached that are in accordance with the solution conductivity (κ). This parameter, which is estimated using the following equation, is presented in Tables 3-5.

$$\kappa = F \sum_j |z_j| \cdot u_j \cdot C_j \tag{9}$$

where C_j is the ion concentration, calculated as explained previously, and whose values are presented in Table SM-1, z_j is the charge of the ion, F is the Faraday's constant and u_j is the mobility of ion j. The values of u_j have been determined from the ionic diffusion coefficient, D_j, using the following equation [44]:

$$u_j(cm^2\ s^{-1}V^{-1}) = \frac{D_j}{R \cdot T} z_j \cdot F \tag{10}$$

where R is the gas constant and T is the temperature. The values of D_j and u_j are presented in Table SM-2 (supplementary material) for all the species under study.

In solution VII (pH=12.44), the predominant species are OH^- ions, whose concentration is $2.75 \cdot 10^{-2}$ M. In this case, since the mobility of the OH^- ions is higher than that of the other anions, the concentration polarization phenomenon was not observed, the membrane potential remains practically constant and coincides with U_{Ohm}. The solutions with pH values of 7.20 and 10.40 have similar U_{Ohm} values since the conductivity of these solutions is similar (see Table SM-2). Finally, the solution with a pH value of 4.79 presents the highest value of U_m because presents the lowest conductivity. Another important aspect is that the transition time increases with pH, i.e., the higher the pH, the longer time required for the complete depletion of the ions in the proximity of the membrane, while the maximum value of the membrane potential, $U_{m,f}$, increases with the decrease in the solution pH.

The solutions whose pH values coincide with the areas of the speciation diagram where only one species clearly predominates, as occurs for solutions I, II, IV, V, X, XI and XII, present the typical chronopotentiograms with only one transition time. However, solutions III, IX and XIII, whose pH is between 6.36 and 7.30, in which several species such as $H_2PO_4^-$ and HPO_4^{2-} predominates, have several transition times as observed in Figure 3 (a) for solution IX (pH=6.36) and in Figure 3 (b) for solution XIII (pH=7.30). When a current is applied, the solution at one of the surfaces of the AEM is desalted, that leads

to an increase in the exclusion of H^+ ions and an increase in the double (triply) charged anions in the membrane. This fact explains why the pH of the micropores of the membrane is higher than the external solution pH, and consequently, the fraction of doubly (triply) charged anions in an AEM is always higher than in the external solution [27].

The occurrence of several transition times in the chronopotentiograms of multicomponent solutions has also been observed by several authors. In this way, Zook et al. [45], who evaluated the transport through a calcium-selective membrane submerged in a solution containing ionophore and calcium cations, found two inflection points in the chonopotentiometric curves: the first one attributed to the transport of free ionophore, and the second one assigned to the ion-ionophore complex transfer. Both inflexion points were completely separated, as a result of the difference in ion mobility and diffusion coefficient. In another work, Scarazzato et al. [42] found two transition times in the chronopotentiometric curves obtained in solutions containing copper ions and etidronic acid in presence of an anion-exchange membrane. They associated the first transition time to the transport of free anions from the dissociation of the etidronic acid, and the second one to the transfer of the chelate formed between the copper ions and the etidronic acid trough the membrane. Martí-Calatayud et al. [46] studying the transport of different metal cation sulfates through a CEM detected the presence of several transition times in the chronopotentiograms which were attributed to the depletion of different ionic species. In other studies [31,33], attributed the presence of the different transition times to the formation of different species as a consequence of the changes in the equilibrium conditions reached in the proximities of the membrane. Finally, Pismenskaya et al. [24] found that the preferential transport of hydroxyl ions may induce pH changes on a membrane surface, and the consequent modification of the transport properties of weak electrolyte anions. This fact led to CVCs with two limiting current densities, corresponding to the transport of ions with different size, molar concentrations, mobility or diffusion coefficients in the membrane matrix. However, in some cases, when the properties of the ions are not very different, only one transition time is observed and a single value of i_{lim} is present in the CVCs, which corresponds to the contribution of all the ions.

Then, the two inflexion points observed in Figure 3 may be explained as a function of the predominant species present in the equilibrium diagrams. In this sense, the first inflexion point observed in Figures 3 (a) and (b) could be related to the depletion of $H_2PO_4^-$ and the second one to the decrease of HPO_4^{2-}. In solutions VI, VII, VIII and XIV, whose pH are between 12.26 and 13.05, HPO_4^{2-} and PO_4^{3-} predominate over the rest of phosphate species; however, in the chronopotentiograms of these solutions, only a transition time is observed (not shown). This transition time corresponds to the depletion of OH^- ions, as in these solutions the OH^- ion concentration is higher than that

of HPO_4^{2-} and PO_4^{3-} ions. Since OH^- ions present the highest mobility, they are primarily removed from the diffusion boundary layer.

Another characteristic of the chronopotentiograms of Figure 3 is the presence of oscillations in U_m at high current densities, which have been usually attributed to the presence of electroconvective vortexes responsible for causing an additional mixing of the depleting boundary layers for i values far above the i_{lim} [47,48].

Figure 4 shows the effect of pH on the CVCs for an initial phosphate concentration of 0.01 M. Regardless of the reagents used to prepare the solutions, for the same total concentration of phosphate ions, and the same pH, similar CVCs were obtained, since pH establishes the concentration of all the species present in the solution. From these curves, the values of R1, i_{lim} and $l_{plateau}$ can be estimated. These values are shown in Table 3, where it is observed that R1 decreases with the solution conductivity estimated by equation (9), and i_{lim} increases with the solution conductivity, as i_{lim} depends on the charge and the concentration of each ion.

In the CVCs of Figure 4 (a) only one plateau was observed, although in the chronopotentiograms obtained at pH values between 6 and 7 two transition times were observed (Figure 3). The presence of the two transition times was previously attributed to the transport of HPO_4^{2-} and $H_2PO_4^-$ across the membrane. As the diffusion coefficients of these species are very similar (see Table SM-2), this fact explains why in the CVCs only one plateau was observed. However, when the CVCs are obtained in potentiodynamic mode, by means of a continuous sweep, it is possible to observe the changes associated with the transport of different species through the membrane. The appearance of two limiting current densities on the CVCs of the AEM in phosphate solutions (0.02 M, pH=4.65) was also observed by Rybalkina et al. [29] and modelled by E.D. Melnikova, et al., [27]. In these works, the first limiting current was attributed to the transport of $H_2PO_4^-$ anions, and the second one to the passage of HPO_4^{2-}, produced by the conversion of $H_2PO_4^-$ as a consequence of the increase in pH.

Figure 4 (b) presents the CVCs for phosphate solutions under very basic pH. The most important feature observed is the large plateaus obtained, which hinders the occurrence of coupled convection phenomena (electroconvection and gravitational convection), and consequently, water splitting can be considered as the main mechanism responsible for the overlimiting regime. In these conditions, OH^- ions are the main species present in solution, and since they are much smaller and mobile than phosphate ions, the initial instabilities of the membrane would be more easily mitigated, hence being necessary the application of stronger electric fields in order to initiate the chaotic distortion of the diffusion boundary layer by the electroconvective vortices. In addition, the abnormal transport properties of hydroxyl ions have also been pointed out

as the reason for the large $I_{plateau}$ values. They are mainly transported by "tunneling" from one water molecule to another according to the Grotthus mechanism, which does not involve the settling of large volumes of fluid in motion. This mechanism will be explained in point 3.4. in more detail.

The CVCs obtained from the chronopotentiograms are compared with the CVCs obtained in potentiodynamic mode for solutions IX (pH = 6.36) and XIII (pH = 7.3) in Figure 5 (a) and (b), respectively. In the CVCs obtained in potentiodynamic mode, several slope changes are observed that correspond to strongly overlapping plateaus in the CVCs from the chronopotentiograms. The shape of these CVCs is similar to that obtained by Pismenscaya et al. [24] when studying the transport of weak-electrolyte anions through anion-exchange membranes.

3.3. Effect of chloride ions.

The effect of a strong electrolyte (such as NaCl) on the transport of the phosphate ions is presented in Table 5 for a phosphate concentration of 0.001 M and 0.0016 M of NaOH, and the corresponding chronopotentiograms are presented in Figure 6.

Table 5. pH, conductivity and CVCs characteristics of the working solutions as a function of the chloride concentration for a phosphate concentration of 0.001 M.

Soln ID	[NaCl] ($mol \cdot L^{-1}$)	pH	κ ($\Omega^{-1} \cdot cm^{-1}$)	R1 ($\Omega \cdot cm^2$)	i_{lim} ($A \cdot cm^{-2}$)	$I_{plateau}$ (V)
XIII	0	7.30	$1.57 \cdot 10^{-4}$	6402	$1.92 \cdot 10^{-5}$	0.90
XV	0.001	7.30	$2.83 \cdot 10^{-4}$	2707	$1.91 \cdot 10^{-4}$	0.90
XVI	0.002	7.30	$4.10 \cdot 10^{-4}$	1608	$2.55 \cdot 10^{-4}$	0.95
XVII	0.005	7.30	$7.89 \cdot 10^{-4}$	864	$6.38 \cdot 10^{-4}$	0.90

For i=0.27 $mA \cdot cm^{-2}$ (Figure 6 (a)) the presence of Cl^- ions in a concentration of 10^{-3} M, causes the decrease of U_m due to the increase of the solution conductivity. In the chronopotentiograms of the solution containing chloride ions, three transition times are observed, which would be related to the transport and successive depletion of Cl^-, $H_2PO_4^-$ and HPO_4^{2-} ions. Since the mobility of Cl^- ions is the highest they are primarily removed. In the absence of chloride ions, only two transition times were observed as discussed in the previous section.

In Figure 6 (b), the effect of chloride concentration on the chronopotentiograms can be observed for i=0.64 mA/cm^2. When the Cl^-/phosphate ratio is greater, the transport of phosphate ions is less evident and the second and third inflexion points are absent. In addition, U_{Ohm} and $U_{m,f}$ decrease with the concentration of Cl^- ions due to the increase in the conductivity of the solutions with the concentration of Cl^- ions.

The effect of Cl^- concentration on the CVCs obtained from the chronopotentiograms can be seen in Figure SM-5 (supplementary material). An increase in the initial chloride concentration leads to higher i_{lim} values. In these curves only one plateau was observed, however, when the CVCs obtained from the chronopotentiograms are compared with those obtained in potentiodynamic mode in Figure SM-5 (b) for the most diluted solution, it is possible to observe several changes in the slope of the CVC obtained in the potentiodynamic sweep. These slope changes in the CVCs would be associated to the transport and depletion of ions with different concentration, charge and diffusion coefficient across the membrane. These slope changes in the CVCs were not observed for the solutions with higher concentrations in chloride ions.

3.4. Effect of the solution composition on the parameters of the CVCs.

As shown above, equation (7) represents the dependence of the i_{lim} as a function of the initial electrolyte concentration (C_0) for a binary system. However, in a multicomponent solution, i is due to the contribution of all the ions present in the solution, and each of the counter ions may be depleted in the membrane surface at a different time, according to its charge, its concentration and its diffusion coefficient. This gives rise to the appearance of different transition times in the chronopotenciograms, or different values of i_{lim} in the CVCs, as previously commented. Therefore, in multicomponent solutions, each counter ion can have its own i_{lim}, and the total limiting current density will be the sum of the limiting current densities of each counter ion, according to the following equations [49]:

$$i_{lim,j} = \frac{FD_j z_j C_j}{\delta}\left(1 + \frac{z_j}{z_A}\right) \tag{11}$$

where $i_{lim,j}$ is the limiting current density of ion j, C_j its concentration, D_j its diffusion coefficient. Index A refers to the common co-ion in the mixed solution containing several counterion species, and z_A is the charge number of this co-ion.

$$i_{lim} = \sum_j i_{lim,j} = \sum_j \frac{FD_j z_j C_j}{\delta}\left(1 + \frac{z_j}{z_A}\right) \tag{12}$$

The limiting current density can be estimated from equation (12) if the other parameters are known. In this sense, the boundary layer thickness has been firstly calculated from equation (8), and the Sc number for multicomponent solutions has been estimated as:

$$Sc = \frac{\nu}{D_{mix}} \tag{13}$$

where D_{mix} is the effective diffusivity of the medium calculated as [50]:

$$\frac{1}{D_{mix}} = \sum_{i=1}^{n} \frac{x_i}{D_{i,self}} \quad (14)$$

x_i is the mol fraction of the component i and $D_{i,self}$ its corresponding diffusion coefficient at infinite dilution. With these assumptions, the limiting current density has been calculated and compared with the measured values in Figure 7, where a very good agreement between the measured and calculated values of i_{lim} is observed.

The plateau length ($l_{plateau}$) depends on the type of electrolyte and membrane [51]. Figure 8 shows the $l_{plateau}$ evolution as a function of the initial concentration of phosphate ions, Figure 8 (a), and pH, Figure 8 (b). As mentioned previously, great values of $l_{plateau}$ enhance the generation of water splitting products whereas low values of $l_{plateau}$ help the coupled phenomena (electroconvection and/or gravitational convection) to take place.

As seen in Figure 8 (a), the plateau length increases with the electrolyte concentration. These results differ from those of other authors; in which $l_{plateau}$ was unaffected by the electrolyte concentration [52,53]. This could be explained by the fact that in those works, binary salts that dissociate completely are considered. On the contrary, in solutions of weak electrolytes, in which hydrolysis reactions take place, the depletion of a given ion in the membrane surface, or the pH changes associated to concentration polarization, may change the equilibrium conditions and new ions or uncharged species can be formed. In Figure 8 (a), the initial pH solution value is about 9, and the predominant species is HPO_4^{2-}. When this anion enters the AEM, part of it is converted into a multicharged anion due to the fact than the internal pH solution is higher than that in the external boundary solution. Consequently, the H^+ ions liberated in this dissociation would react with the HPO_4^{2-} to transform it into less charged ions such as $H_2PO_4^-$ or H_3PO_4. and the voltage necessary for the depletion of these ions would be higher. This effect would be more pronounced at higher initial electrolyte concentrations. Hence, the decrease in the plateau length at low concentrations facilitates the appearance of electroconvection. This phenomenon is responsible for the oscillations of U_m observed in the chronopotenciograms of the most diluted solutions shown in Figure 3.

The effect of pH on the plateau length for an initial concentration of 0.01 M in phosphate ions is shown in Figure 8 (b). For a constant concentration of phosphate ions, $l_{plateau}$ remains almost constant until a pH value of 9.5, and beyond pH 10, it increases with pH. This is due to the fact that at high pH values, OH^- ions predominate over the other species in solution. In addition, as OH^- is the anion with the greatest mobility, its contribution to the transport through the membrane at high pH values is the highest. In

this way, electroconvection and gravitational convection phenomena were only observed at low OH^- concentrations.

The effect OH^- ion concentration on the plateau length observed in anion-exchange membranes is similar to the effect of H^+ ions on the plateau length in cation-exchange membranes at low pH values. Some authors have found that the plateau length becomes higher as the H^+ ion concentration increases [33,52], because the size of the counterion is so small that it is necessary the application of stronger electric fields in order to initiate the electroconvection vortices. On the other hand, protons are mainly transported by the Grotthus mechanism [54], and it does not imply the fluid movement, and the consequent electroconvection phenomena.

Wang et al. and Chen et al. [55,56] have also found that the transport mechanism of OH^- in AEMs is the same as the transport of H^+ in cation-exchange membranes. According to these authors, the OH^- diffusion likely combines both the mass diffusion and Grotthuss mechanisms in the hydrated membranes. Then, the increase of the plateau length observed can be attributed to the transport mechanism of OH^- ions across the AEM. In addition, the OH^- ions expulse salt counterions, which hinders electroconvection [57–59]. Therefore, the resistance of the membrane system keeps high until new higher electric field are applied.

4. Conclusions.

In this work, the transport properties of salts of orthophosphoric acid through an anion-exchange membrane at different concentrations of phosphate salts or chloride ions, and pH values were studied by means of chronopotentiometry and CVCs. The transport properties depended on the solution pH due to the hydrolysis reactions which change the concentration of the different species in the solution.

An increase of the concentration value of Na_2HPO_4 (0.1 M) for applied currents higher than $i_{lim,}$ was reflected by a maximum in U_m after the transition time attributed to the decrease of the concentration polarization phenomena caused by different phenomena such as the transfer of co-ions across the membrane, which increases with time during chronopotentiometry, together with the gravitational convection, which can take place in concentrated electrolytes.

At pH values close to a pK_j, and when the concentration of OH^- ions is not significant, at least two species have similar concentrations. In these cases, the chronopotentiograms showed several transition times and the CVCs presented different waves. This was due to the successive transfer of species with different charge and mobilities across the membrane. However, at high pH values, only one transition time in the chronopotentiograms, that is mainly due to the transfer of OH^- ions due to their greater concentration and mobility. The most important feature observed in the CVCs under very basic pH is the large plateaus obtained, which hinders the occurrence of coupled convection phenomena (electroconvection and gravitational convection), and consequently, water splitting can be considered as the main mechanism responsible for the overlimiting regime.

The transport properties were affected by the concentration, charge and mobility of each ion present in the solution. The limiting current density calculated taking into account the contribution of all the ions of the solution was compared with the limiting current density measured from the CVCs, and a very good agreement between both values were obtained.

In solutions with similar pH values, the plateau length increased with the initial salt concentration. Moreover, in solutions with the same salt concentration, the plateau length remained almost constant with pH up to a pH value around 9. Beyond this pH value, the plateau length increased with the pH due to the presence of OH^- ions.

Acknowledgments.

The authors wish to thank the financial support from FINEP, FAPERGS, CAPES and CNPq (Brazil), from the BRICS-STI/CNPq (BRICS STI Framework Programme), from the European Union through the Erasmus Mundus Program (EBW+) and from the CYTED (Network 318RT0551).

References.

[1] D. Cordell, J.-O. Drangert, S. White, The story of phosphorus: Global food security and food for thought, Glob. Environ. Chang. 19 (2009) 292–305. doi:10.1016/J.GLOENVCHA.2008.10.009.

[2] D. Cordell, A. Rosemarin, J.J. Schröder, A.L. Smit, Towards global phosphorus security: A systems framework for phosphorus recovery and reuse options, Chemosphere. 84 (2011) 747–758. doi:10.1016/j.chemosphere.2011.02.032.

[3] D.P. Van Vuuren, A.F. Bouwman, A.H.W. Beusen, Phosphorus demand for the 1970–2100 period: A scenario analysis of resource depletion, Glob. Environ. Chang. 20 (2010) 428–439. doi:10.1016/J.GLOENVCHA.2010.04.004.

[4] N. Gilbert, Environment: The disappearing nutrient, Nature. 461 (2009) 716–718. doi:10.1038/461716a.

[5] X. Hao, C. Wang, M.C.M. van Loosdrecht, Y. Hu, Looking Beyond Struvite for P-Recovery, Environ. Sci. Technol. 47 (2013) 4965–4966. doi:10.1021/es401140s.

[6] M. Arnaldos, K. Pagilla, Effluent dissolved organic nitrogen and dissolved phosphorus removal by enhanced coagulation and microfiltration, Water Res. 44 (2010) 5306–5315. doi:10.1016/J.WATRES.2010.06.066.

[7] A.O. Babatunde, Y.Q. Zhao, Equilibrium and kinetic analysis of phosphorus adsorption from aqueous solution using waste alum sludge, J. Hazard. Mater. 184 (2010) 746–752. doi:10.1016/J.JHAZMAT.2010.08.102.

[8] R.P. Kralchevska, R. Prucek, J. Kolařík, J. Tuček, L. Machala, J. Filip, V.K. Sharma, R. Zbořil, Remarkable efficiency of phosphate removal: Ferrate(VI)-induced in situ sorption on core-shell nanoparticles, Water Res. 103 (2016) 83–91. doi:10.1016/J.WATRES.2016.07.021.

[9] C. Maher, J.B. Neethling, S. Murthy, K. Pagilla, Kinetics and capacities of phosphorus sorption to tertiary stage wastewater alum solids, and process implications for achieving low-level phosphorus effluents, Water Res. 85 (2015) 226–234. doi:10.1016/J.WATRES.2015.08.025.

[10] K. Furuya, A. Hafuka, M. Kuroiwa, H. Satoh, Y. Watanabe, H. Yamamura, Development of novel polysulfone membranes with embedded zirconium sulfate-surfactant micelle mesostructure for phosphate recovery from water through membrane filtration, Water Res. 124 (2017) 521–526. doi:10.1016/J.WATRES.2017.08.005.

[11] Y. Zhang, E. Desmidt, A. Van Looveren, L. Pinoy, B. Meesschaert, B. Van der Bruggen, Phosphate Separation and Recovery from Wastewater by Novel Electrodialysis, Environ. Sci. Technol. 47 (2013) 5888–5895. doi:10.1021/es4004476.

[12] B. Valverde-Pérez, D.S. Wágner, B. Lóránt, A. Gülay, B.F. Smets, B.G. Plósz, Short-sludge age EBPR process – Microbial and biochemical process characterisation during reactor start-up and operation, Water Res. 104 (2016) 320–329. doi:10.1016/J.WATRES.2016.08.026.

[13] X. Chen, H. Zhou, K. Zuo, Y. Zhou, Q. Wang, D. Sun, Y. Gao, P. Liang, X. Zhang, Z.J. Ren, X. Huang, Self-sustaining advanced wastewater purification and simultaneous in situ nutrient recovery in a novel bioelectrochemical system, Chem. Eng. J. 330 (2017) 692–697. doi:10.1016/J.CEJ.2017.07.130.

[14] K.S. Le Corre, E. Valsami-Jones, P. Hobbs, S.A. Parsons, Phosphorus Recovery

from Wastewater by Struvite Crystallization: A Review, Crit. Rev. Environ. Sci. Technol. 39 (2009) 433–477. doi:10.1080/10643380701640573.
[15] Y. Ueno, M. Fujii, Three Years Experience of Operating and Selling Recovered Struvite from Full-Scale Plant, Environ. Technol. 22 (2001) 1373–1381. doi:10.1080/09593332208618196.
[16] P. Battistoni, R. Boccadoro, F. Fatone, P. Pavan, Auto-Nucleation and Crystal Growth of Struvite in a Demonstrative Fluidized Bed Reactor (FBR), Environ. Technol. 26 (2005) 975–982. doi:10.1080/09593332608618486.
[17] R. Liu, Y. Wang, G. Wu, J. Luo, S. Wang, Development of a selective electrodialysis for nutrient recovery and desalination during secondary effluent treatment, Chem. Eng. J. 322 (2017) 224–233. doi:10.1016/J.CEJ.2017.03.149.
[18] S. Ren, M. Li, J. Sun, Y. Bian, K. Zuo, X. Zhang, P. Liang, X. Huang, A novel electrochemical reactor for nitrogen and phosphorus recovery from domestic wastewater, Front. Environ. Sci. Eng. 11 (2017) 17. doi:10.1007/s11783-017-0983-x.
[19] Y. Wimalasiri, M. Mossad, L. Zou, Thermodynamics and kinetics of adsorption of ammonium ions by graphene laminate electrodes in capacitive deionization, Desalination. 357 (2015) 178–188. doi:10.1016/J.DESAL.2014.11.015.
[20] G.-H. Huang, T.-C. Chen, S.-F. Hsu, Y.-H. Huang, S.-H. Chuang, Capacitive deionization (CDI) for removal of phosphate from aqueous solution, Desalin. Water Treat. 52 (2014) 759–765. doi:10.1080/19443994.2013.826331.
[21] X. Wang, Y. Wang, X. Zhang, H. Feng, C. Li, T. Xu, Phosphate Recovery from Excess Sludge by Conventional Electrodialysis (CED) and Electrodialysis with Bipolar Membranes (EDBM), Ind. Eng. Chem. Res. 52 (2013) 15896–15904. doi:10.1021/ie4014088.
[22] B. Ebbers, L.M. Ottosen, P.E. Jensen, Electrodialytic treatment of municipal wastewater and sludge for the removal of heavy metals and recovery of phosphorus, Electrochim. Acta. 181 (2015) 90–99. doi:10.1016/J.ELECTACTA.2015.04.097.
[23] M.C. Martí-Calatayud, E. Evdochenko, J. Bär, M. García-Gabaldón, M. Wessling, V. Pérez-Herranz, Tracking homogeneous reactions during electrodialysis of organic acids via EIS, J. Memb. Sci. (2019) 117592. doi:10.1016/J.MEMSCI.2019.117592.
[24] N. Pismenskaya, V. Nikonenko, B. Auclair, G. Pourcelly, Transport of weak-electrolyte anions through anion exchange membranes: Current–voltage characteristics, J. Memb. Sci. 189 (2001) 129–140. doi:10.1016/S0376-7388(01)00405-7.
[25] E.D. Belashova, O.A. Kharchenko, V. V. Sarapulova, V. V. Nikonenko, N.D. Pismenskaya, Effect of Protolysis Reactions on the Shape of Chronopotentiograms of a Homogeneous Anion-Exchange Membrane in NaH_2PO_4 Solution, Pet. Chem. 57 (2017) 1207–1218. doi:10.1134/S0965544117130035.
[26] E.D. Belashova, N.D. Pismenskaya, V.V. Nikonenko, P. Sistat, G. Pourcelly, Current-voltage characteristic of anion-exchange membrane in monosodium phosphate solution. Modelling and experiment, J. Memb. Sci. 542 (2017) 177–185. doi:10.1016/J.MEMSCI.2017.08.002.
[27] E.D. Melnikova, N.D. Pismenskaya, L. Bazinet, S. Mikhaylin, V. V. Nikonenko,

Effect of ampholyte nature on current-voltage characteristic of anion-exchange membrane, Electrochim. Acta. 285 (2018) 185–191. doi:10.1016/j.electacta.2018.07.186.

[28] L. Paltrinieri, L. Poltorak, L. Chu, T. Puts, W. van Baak, E.J.R. Sudhölter, L.C.P.M. de Smet, Hybrid polyelectrolyte-anion exchange membrane and its interaction with phosphate, React. Funct. Polym. 133 (2018) 126–135. doi:10.1016/J.REACTFUNCTPOLYM.2018.10.005.

[29] O. Rybalkina, K. Tsygurina, E. Melnikova, S. Mareev, I. Moroz, V. Nikonenko, N. Pismenskaya, Partial Fluxes of Phosphoric Acid Anions through Anion-Exchange Membranes in the Course of NaH2PO4 Solution Electrodialysis, Int. J. Mol. Sci. 20 (2019) 3593. doi:10.3390/ijms20143593.

[30] M.C. Martí-Calatayud, D.C. Buzzi, M. García-Gabaldón, A.M. Bernardes, J.A.S. Tenório, V. Pérez-Herranz, Ion transport through homogeneous and heterogeneous ion-exchange membranes in single salt and multicomponent electrolyte solutions, J. Memb. Sci. 466 (2014) 45–57. doi:10.1016/j.memsci.2014.04.033.

[31] T. Benvenuti, M. García-Gabaldón, E.M. Ortega, M.A.S. Rodrigues, A.M. Bernardes, V. Pérez-Herranz, J. Zoppas-Ferreira, Influence of the co-ions on the transport of sulfate through anion exchange membranes, J. Memb. Sci. 542 (2017) 320–328. doi:10.1016/j.memsci.2017.08.021.

[32] P. Ray, V.K. Shahi, T. V. Pathak, G. Ramachandraiah, Transport phenomenon as a function of counter and co-ions in solution: Chronopotentiometric behavior of anion exchange membrane in different aqueous electrolyte solutions, J. Memb. Sci. 160 (1999) 243–254. doi:10.1016/S0376-7388(99)00088-5.

[33] M.C. Martí-Calatayud, M. García-Gabaldón, V. Pérez-Herranz, E. Ortega, Determination of transport properties of Ni(II) through a Nafion cation-exchange membrane in chromic acid solutions, J. Memb. Sci. 379 (2011) 449–458. doi:10.1016/j.memsci.2011.06.014.

[34] L. Marder, E.M. Ortega Navarro, V. Pérez-Herranz, A.M. Bernardes, J.Z. Ferreira, Evaluation of transition metals transport properties through a cation-exchange membrane by chronopotentiometry, J. Memb. Sci. 284 (2006). doi:10.1016/j.memsci.2006.07.039.

[35] I. Herraiz-Cardona, E. Ortega, V. Pérez-Herranz, Evaluation of the Zn^{2+} transport properties through a cation-exchange membrane by chronopotentiometry, J. Colloid Interface Sci. 341 (2010) 380–385. doi:10.1016/j.jcis.2009.09.053.

[36] M.C. Martí-Calatayud, M. García-Gabaldón, V. Pérez-Herranz, Study of the effects of the applied current regime and the concentration of chromic acid on the transport of Ni^{2+} ions through Nafion 117 membranes, J. Memb. Sci. 392–393 (2012) 137–149. doi:10.1016/j.memsci.2011.12.012.

[37] N. Pismenskaia, P. Sistat, P. Huguet, V. Nikonenko, G. Pourcelly, Chronopotentiometry applied to the study of ion transfer through anion exchange membranes, J. Memb. Sci. 228 (2004) 65–76. doi:10.1016/J.MEMSCI.2003.09.012.

[38] M. Taky, G. Pourcelly, F. Lebon, C. Gavach, Polarization phenomena at the interfaces between an electrolyte solution and an ion exchange membrane: Part I. Ion transfer with a cation exchange membrane, J. Electroanal. Chem. 336 (1992) 171–194. doi:10.1016/0022-0728(92)80270-E.

[39] V. V. Nikonenko, N.D. Pismenskaya, E.I. Belova, P. Sistat, P. Huguet, G. Pourcelly, C. Larchet, Intensive current transfer in membrane systems: Modelling, mechanisms and application in electrodialysis, Adv. Colloid Interface Sci. 160 (2010) 101–123. doi:10.1016/J.CIS.2010.08.001.
[40] J.J. Krol, M. Wessling, H. Strathmann, Concentration polarization with monopolar ion exchange membranes: current–voltage curves and water dissociation, J. Memb. Sci. 162 (1999) 145–154. doi:10.1016/S0376-7388(99)00133-7.
[41] C. Larchet, S. Nouri, B. Auclair, L. Dammak, V. Nikonenko, Application of chronopotentiometry to determine the thickness of diffusion layer adjacent to an ion-exchange membrane under natural convection, Adv. Colloid Interface Sci. 139 (2008) 45–61. doi:10.1016/J.CIS.2008.01.007.
[42] T. Scarazzato, Z. Panossian, M. García-Gabaldón, E.M. Ortega, J.A.S. Tenório, V. Pérez-Herranz, D.C.R. Espinosa, Evaluation of the transport properties of copper ions through a heterogeneous ion-exchange membrane in etidronic acid solutions by chronopotentiometry, J. Memb. Sci. 535 (2017). doi:10.1016/j.memsci.2017.04.048.
[43] V.G. Levich, Physicochemical Hydrodynamics, Prentice-Hall, Englewood Cliffs, NJ, 1962.
[44] D.R. Lide, CRC Handbook of Chemistry and Physics, 70th ed., CRC Press Inc., Boca Raton, 2009.
[45] J.M. Zook, S. Bodor, R.E. Gyurcsányi, E. Lindner, Interpretation of chronopotentiometric transients of ion-selective membranes with two transition times, J. Electroanal. Chem. 638 (2010) 254–261. doi:10.1016/J.JELECHEM.2009.11.007.
[46] M.C. Martí-Calatayud, M. García-Gabaldón, V. Pérez-Herranz, Effect of the equilibria of multivalent metal sulfates on the transport through cation-exchange membranes at different current regimes, J. Memb. Sci. 443 (2013). doi:10.1016/j.memsci.2013.04.058.
[47] F. Maletzki, H.-W. Rösler, E. Staude, Ion transfer across electrodialysis membranes in the overlimiting current range: stationary voltage current characteristics and current noise power spectra under different conditions of free convection, J. Memb. Sci. 71 (1992) 105–116. doi:10.1016/0376-7388(92)85010-G.
[48] Elena I. Belova, Galina Yu. Lopatkova, Natalia D. Pismenskaya, Victor V. Nikonenko, and Christian Larchet, G. Pourcelly, Effect of Anion-exchange Membrane Surface Properties on Mechanisms of Overlimiting Mass Transfer, (2006). doi:10.1021/JP062433F.
[49] V. V. Nikonenko, A. V. Kovalenko, M.K. Urtenov, N.D. Pismenskaya, J. Han, P. Sistat, G. Pourcelly, Desalination at overlimiting currents: State-of-the-art and perspectives, Desalination. 342 (2014) 85–106. doi:10.1016/j.desal.2014.01.008.
[50] X. Liu, T.J.H. Vlugt, A.E. Bardow, Predictive Darken Equation for Maxwell-Stefan Diffusivities in Multicomponent Mixtures, Ind. Eng. Chem. Res. 50 (2011) 10350–10358. doi:10.1021/ie201008a.
[51] A. Elattar, A. Elmidaoui, N. Pismenskaia, C. Gavach, G. Pourcelly, Comparison of transport properties of monovalent anions through anion-exchange membranes, J. Memb. Sci. 143 (1998) 249–261. doi:10.1016/S0376-

7388(98)00013-1.
[52] J.-H. Choi, H.-J. Lee, S.-H. Moon, Effects of Electrolytes on the Transport Phenomena in a Cation-Exchange Membrane, J. Colloid Interface Sci. 238 (2001) 188–195. doi:10.1006/JCIS.2001.7510.
[53] I. Rubinstein, B. Zaltzman, Electro-osmotically induced convection at a permselective membrane, Phys. Rev. E - Stat. Physics, Plasmas, Fluids, Relat. Interdiscip. Top. 62 (2000) 2238–2251. doi:10.1103/PhysRevE.62.2238.
[54] N. Agmon, The Grotthuss mechanism, Chem. Phys. Lett. 244 (1995) 456–462. doi:10.1016/0009-2614(95)00905-J.
[55] C. Chen, Y.-L.S. Tse, G.E. Lindberg, C. Knight, G.A. Voth, Hydroxide Solvation and Transport in Anion Exchange Membranes, J. Am. Chem. Soc. 138 (2016) 991–1000. doi:10.1021/jacs.5b11951.
[56] C. Wang, B. Mo, Z. He, X. Xie, C.X. Zhao, L. Zhang, Q. Shao, X. Guo, E.K. Wujcik, Z. Guo, Hydroxide ions transportation in polynorbornene anion exchange membrane, Polymer (Guildf). 138 (2018) 363–368. doi:10.1016/J.POLYMER.2018.01.079.
[57] N.D. Pismenskaya, V. V. Nikonenko, E.I. Belova, G.Y. Lopatkova, P. Sistat, G. Pourcelly, K. Larshe, Coupled convection of solution near the surface of ion-exchange membranes in intensive current regimes, Russ. J. Electrochem. 43 (2007) 307–327. doi:10.1134/S102319350703010X.
[58] N.D. Pismenskaya, V. V. Nikonenko, N.A. Melnik, G. Pourcelli, G. Larchet, Effect of the ion-exchange-membrane/solution interfacial characteristics on the mass transfer at severe current regimes, Russ. J. Electrochem. 48 (2012) 610–628. doi:10.1134/S1023193512060092.
[59] E. Belova, G. Lopatkova, N. Pismenskaya, V. Nikonenko, C. Larchet, Role of water splitting in development of electroconvection in ion-exchange membrane systems, Desalination. 199 (2006) 59–61. doi:10.1016/j.desal.2006.03.142.

LIST OF TABLES.

LIST OF FIGURES.

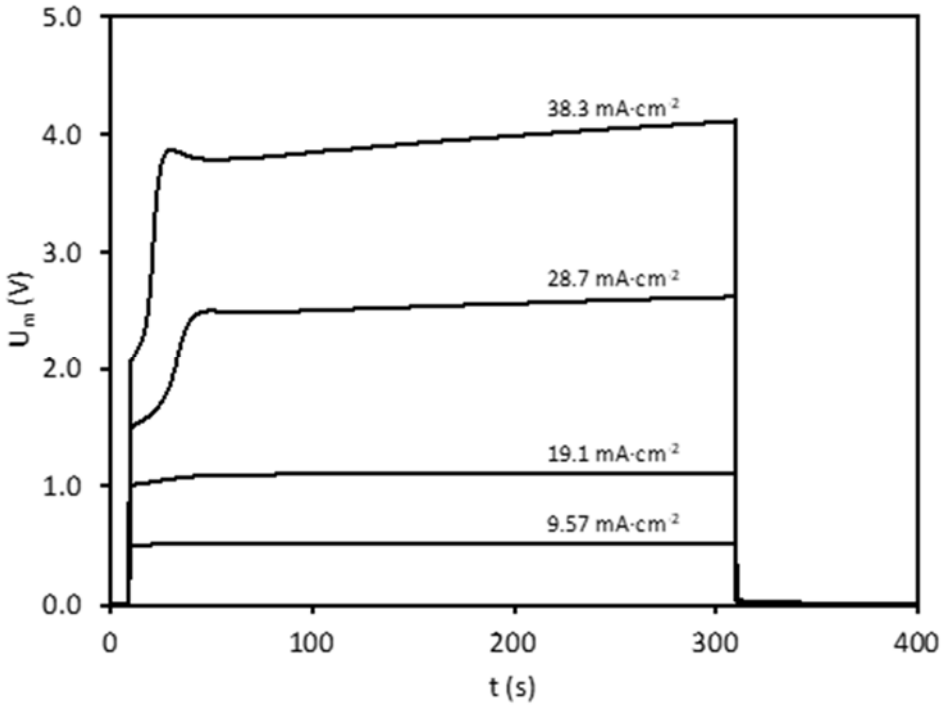

Figure 1. Chronopotentiograms obtained for 0.1 mol·L^{-1} Na_2HPO_4 solutions.

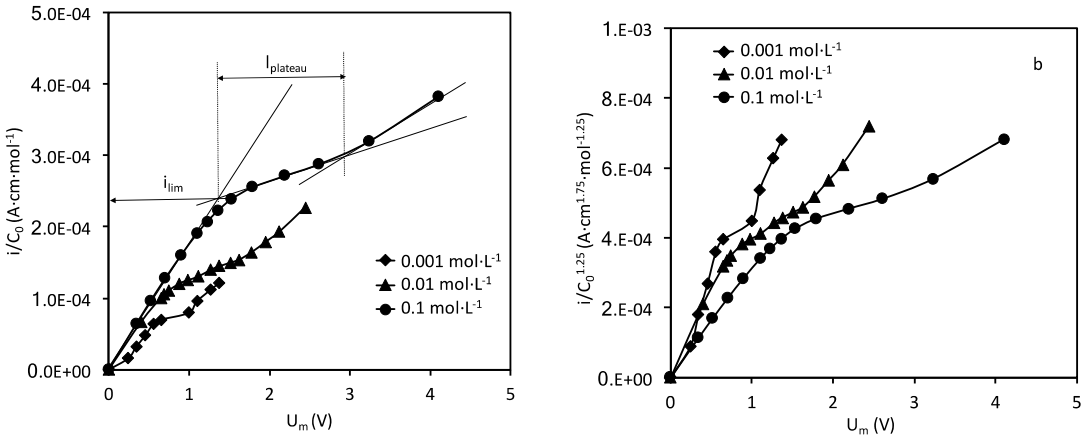

Figure 2. Effect of Na_2HPO_4 concentration on the CVCs corrected with respect to C_0 (a) and to $C_0^{1.25}$ (b). falta letra a

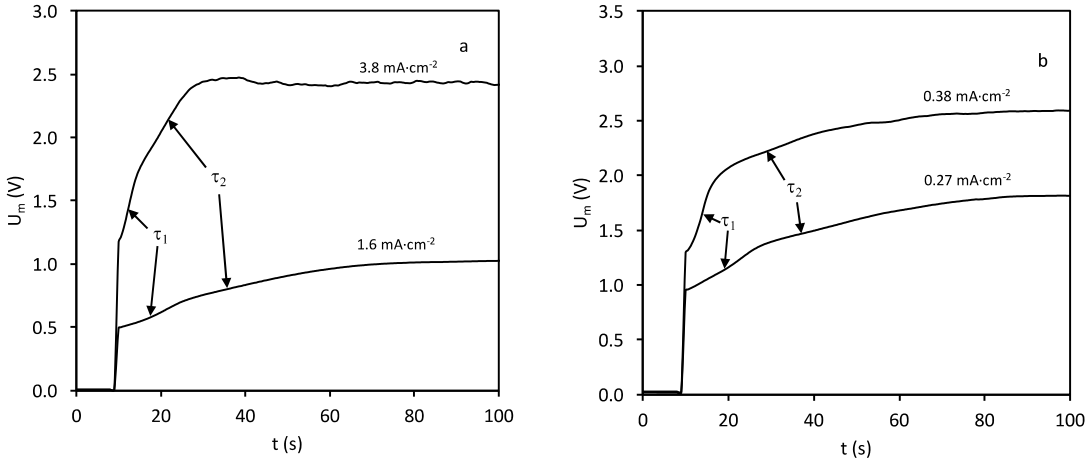

Figure 3. Chronopotentiograms of a 0.01 M phosphate solution at pH 6.36 (a) and of a 0.001 M phosphate solution at pH 7.30 (b).

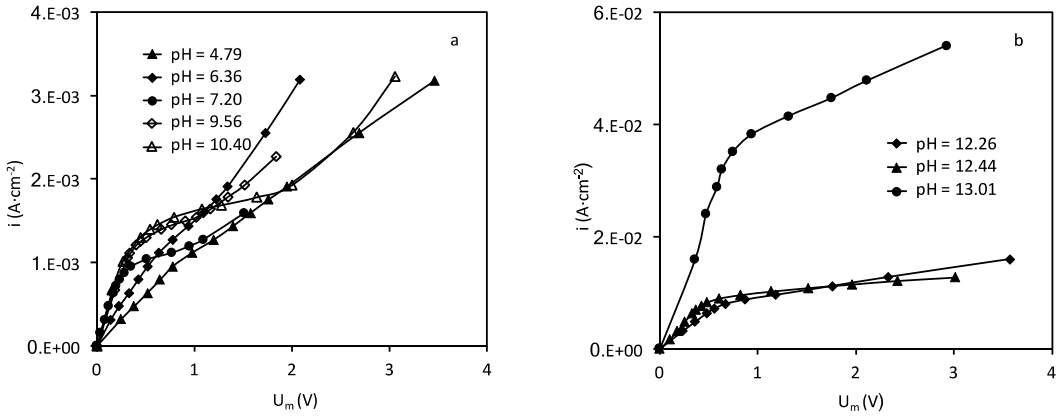

Figure 4. Effect of pH on the CVCs for a solution 0.01 M in phosphate.

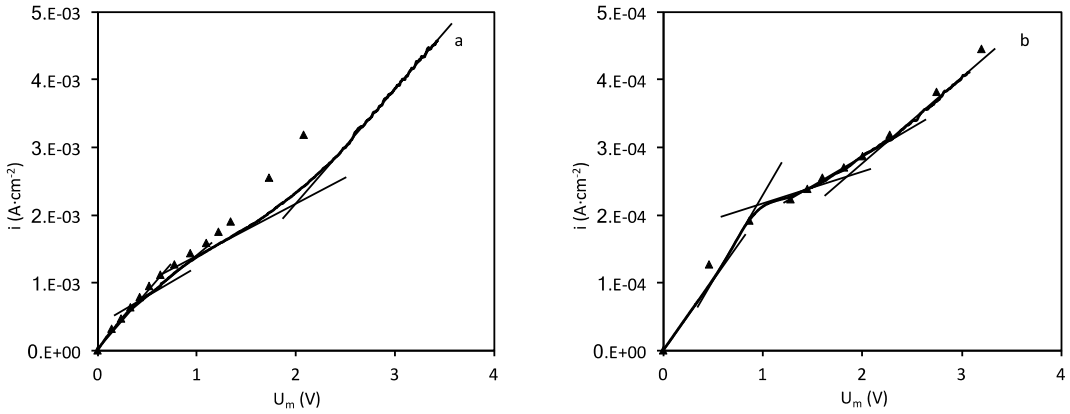

Figure 5. CVCs of solutions IX (a) and XIII (b). Dots: CVC obtained from chronopotentiograms. Continuous line: CVC obtained potentiodynamically.

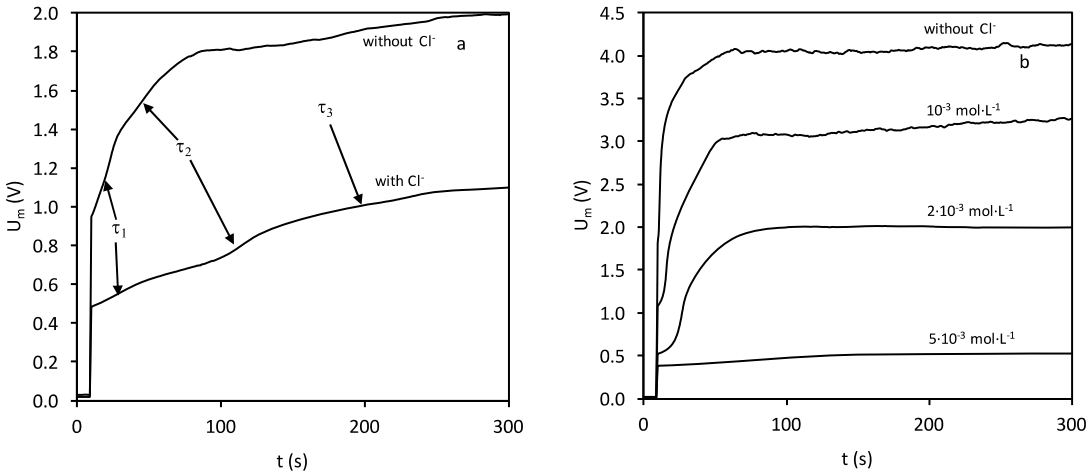

Figure 6. Effect of chloride concentration on the chronopotentiograms of a 0.001 M phosphate solution at pH 7.30. (a) applied current density of 0.27 mA·cm^{-2}. (b) applied current density of 0.64 mA·cm^{-2}.

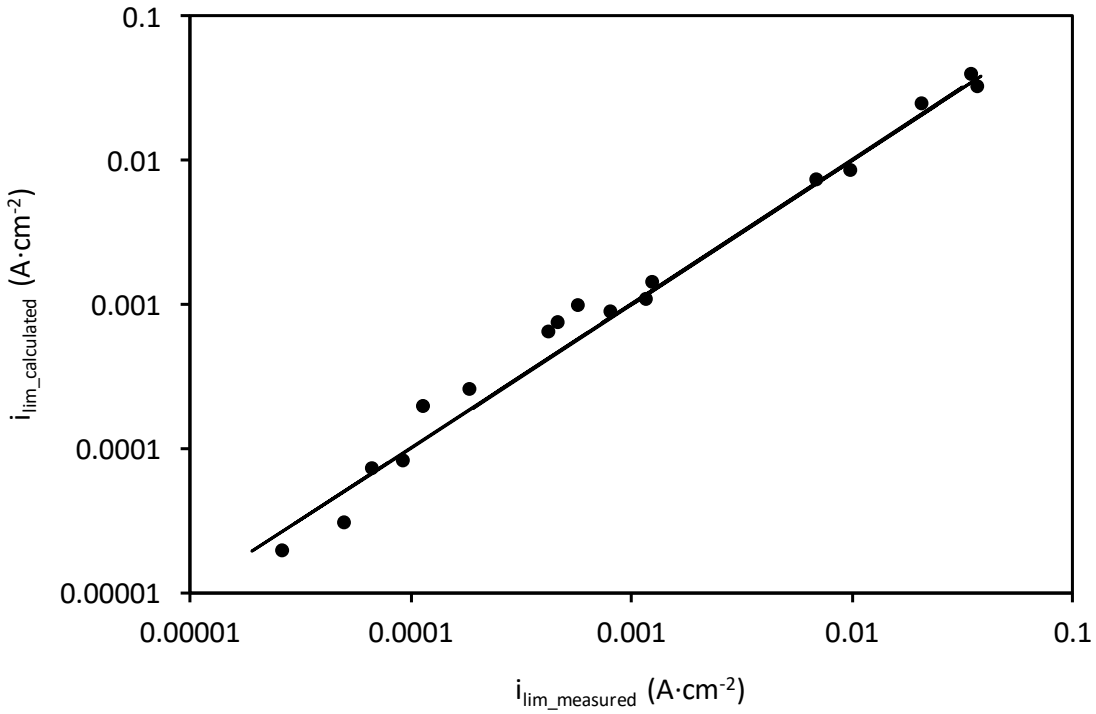

Figure 7. Comparison between i_{lim} obtained experimentally and calculated by equation (12).

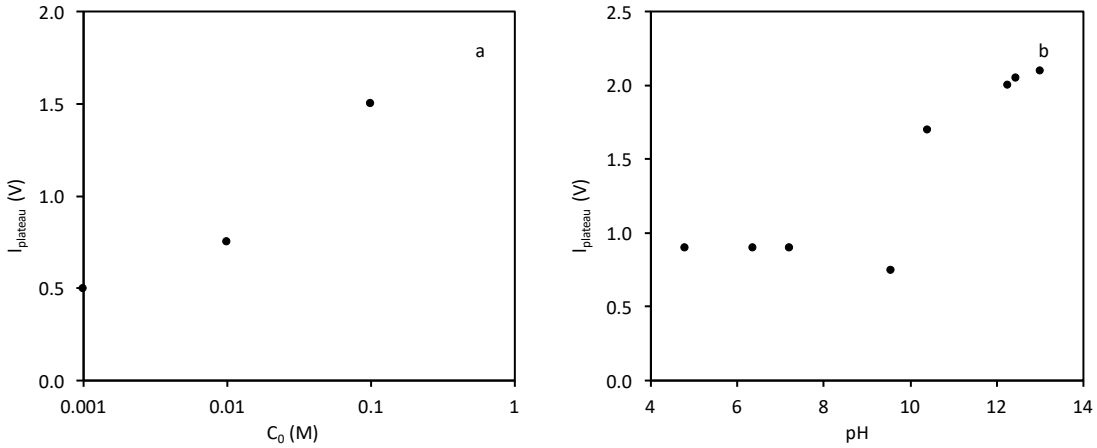

Figure 8. Effect of the initial phosphate concentration (a) and the pH (b) on the plateau length.